



# Fabrication of Fluorescence Turn-off-on Sensor Based on g-C<sub>3</sub>N<sub>4</sub> Quantum Dots and MgFe Layered Double Hydroxide for the Detection of Citrate

Qiao Cheng<sup>1</sup> · Xinyi Liu<sup>1</sup> · Yu He<sup>1,2</sup> · Yili Ge<sup>1</sup> · Jiangang Zhou<sup>2</sup> · Gongwu Song<sup>1</sup>

Received: 1 March 2019 / Accepted: 6 May 2019 / Published online: 16 May 2019  
© Springer Science+Business Media, LLC, part of Springer Nature 2019

## Abstract

We fabricated a new and selective fluorescent sensor for the detection of citrate by employing g-C<sub>3</sub>N<sub>4</sub> quantum dots (g-CNQDs) and MgFe layered double hydroxide (MgFe-LDH). The g-CNQDs interacted with MgFe-LDH via electrostatic interaction and the fluorescence of g-CNQDs was effectively quenched by MgFe-LDH due to inner filter effect. Upon addition of citrate, the fluorescence of the g-CNQDs was significantly enhanced, arising from the replacement of g-CNQDs by citrate because citrate competed with g-CNQDs to form more stable complexes with MgFe-LDH. Therefore, we developed a “turn-off-on” fluorescence assay method for the detection of citrate. This method enabled the selective detection of citrate with linear range of 0.5–3.0 μM and 3.0–10.0 μM with a 12.3 nM limit of detection. This method exhibited advantages including easy preparation, environmentally friendly process and rapid response toward citrate.

**Keywords** G-CNQDs · Layered double hydroxide · Citrate · Fluorescence · Turn-off-on

## Introduction

Citrate is one of the most important anions due to its vital role in the Krebs cycle, which plays the essential roles in metabolism of aerobic organisms [1–3]. Measurements of citrate can lead to a better understanding of certain pathological state, for instance, the reduction of citrate in urine associated with kidney dysfunction [4–6]. It has been reported that citrate levels are as low as 2–20 mM in prostate cancer, while those in healthy males are 50–200 mM. To date, conventional methods have been used for citrate detection include ion chromatography [7, 8], high per-

formance liquid chromatography [9], gas chromatography [10] and spectrometry [11, 12]. However, these methods usually involve specialized and expensive equipment, complicated sample pretreatment and time consuming. Recently, fluorescence methods have been explored in the sensing of citrate, which has the advantages of easy operation, fast response and high sensitivity [13–18]. In general, these methods could be achieved for detection of citrate through two typical avenues: binding with metal cations or complexation with the pyridinium, which are subjected to complex preparation or lower selectivity. Therefore, the development of simple, fast and selective methods for citrate detection is of great significance.

Graphitic carbon nitride (g-C<sub>3</sub>N<sub>4</sub>) has been widely applied in energy, medicine, cell imaging and sensing [19–22]. Especially, g-C<sub>3</sub>N<sub>4</sub> quantum dots (g-CNQDs) have attracted a great deal of attention due to their high fluorescence quantum yields, heavy-metal free structure, high biocompatibility and low toxicity. The characteristics have placed g-CNQDs as fluorophores for the design of probes for biological and environmental molecular species detection. However, most of g-CNQDs based fluorescence probes were focused on the determination of metal ions and biothiols [23–26]. Therefore, it is highly desirable to design g-C<sub>3</sub>N<sub>4</sub>-based sensors to further expand the application range.

✉ Yu He  
heyu@hubu.edu.cn

Jiangang Zhou  
43160562@qq.com

<sup>1</sup> Hubei Collaborative Innovation Center for Advanced Organic Chemical Materials, Ministry-of-Education Key Laboratory for the Synthesis and Application of Organic Functional Molecules, College of Chemistry and Chemical Engineering, Hubei University, Wuhan 430062, China

<sup>2</sup> Hubei Province Key Laboratory of Regional Development and Environment Response, Wuhan 430062, China

Layered double hydroxide (LDH), as one of the most promising two-dimensional nanostructured materials, consisting of a positively charged layer and exchangeable anions in the interlayer [27]. Due to the unique structural properties and ability to assemble with other functional materials, as well as being easy for synthesis, non-toxic, good biocompatible and inexpensive, use of LDH as a component of sensor has recently been proposed [28–32]. LDH has been explored as nanoreactor to provide a stable microenvironment and acted as the disperse matrix to control the distribution of intercalated fluorescence guest [29, 30]. In addition, LDH has been used to fabricate ultrathin films with other fluorescence materials to improve the fluorescence intensity resulted from the localization and confinement effects of LDH nanosheets [31, 32].

Recently, to get more reliable analytical results and better sensitivity, turn-off-on fluorescence probes based on nanoquenching materials such as  $\text{MnO}_2$ ,  $\text{CoOOH}$  and  $\text{AgNPs}$  have been used for analytical testing [33–35]. Herein, we design a novel and selective fluorescent assay for the detection of citrate with  $\text{MgFe-LDH}$  as the nanoquencher. The principle of this strategy is demonstrated in Scheme 1. The fluorescence of  $\text{g-CNQDs}$  can be quenched by  $\text{MgFe-LDH}$  via an inner filter effect. Citrate competes with  $\text{g-CNQDs}$  to form fairly stable complexes with  $\text{MgFe-LDH}$  through intercalation. This results in the replacement of  $\text{g-CNQDs}$  by citrate and fluorescence recovery, allowing quantitative analysis of citrate. This  $\text{g-CNQDs}$ -based method for the detection was designed for the first time. The assay method demonstrates easy preparation, environmentally friendly process and rapid response toward citrate.

## Experimental Section

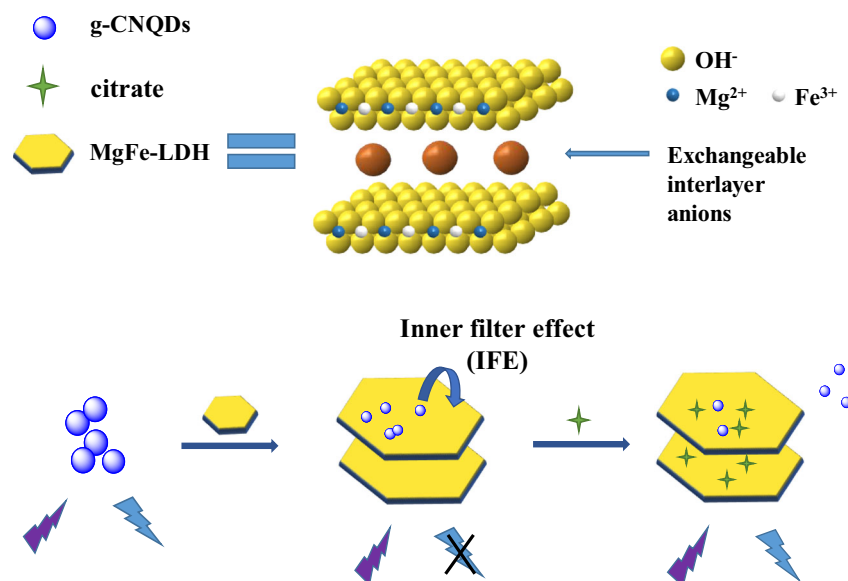
### Reagents

Melamine ( $\text{C}_3\text{N}_6\text{H}_6$ ) and sodium formate ( $\text{HCOONa}$ ) were purchased from Macklin Biochemical Technology Co., Ltd. (Shanghai, China). Ethylene diamine tetraacetic acid (EDTA), sodium hydroxide ( $\text{NaOH}$ ), magnesium chloride hexahydrate ( $\text{MgCl}_2 \cdot 6\text{H}_2\text{O}$ ), ferric chloride hexahydrate ( $\text{FeCl}_3 \cdot 6\text{H}_2\text{O}$ ), potassium bromide ( $\text{KBr}$ ), Potassium iodide ( $\text{KI}$ ), sodium fluoride ( $\text{NaF}$ ), sodium sulfate ( $\text{Na}_2\text{SO}_4$ ), sodium silicate ( $\text{Na}_2\text{SiO}_3$ ), sodium acetate anhydrous ( $\text{CH}_3\text{COONa} \cdot 3\text{H}_2\text{O}$ ), potassium sodium tartrate tetrahydrate ( $\text{KNaC}_4\text{H}_4\text{O}_6 \cdot 4\text{H}_2\text{O}$ ), monopotassium phosphate ( $\text{KH}_2\text{PO}_4$ ) and disodium hydrogen phosphate ( $\text{Na}_2\text{HPO}_4$ ) were purchased from Sinopharm Chemical Reagent Co., Ltd. (Shanghai, China). Potassium Chloride ( $\text{KCl}$ ), sodium nitrate ( $\text{NaNO}_3$ ), sodium carbonate ( $\text{Na}_2\text{CO}_3$ ), sodium sulfite ( $\text{Na}_2\text{SO}_3$ ) and sodium citrate ( $\text{Na}_3\text{C}_6\text{H}_5\text{O}_7 \cdot 2\text{H}_2\text{O}$ ) were purchased from Bodi Chemical Co., Ltd. (Tianjin, China). Sodium oxalate ( $\text{Na}_2\text{C}_2\text{O}_4$ ) was purchased from Kermel Chemical Reagent Co., Ltd. (Tianjin, China).

### Instruments

Transmission electron microscopy (TEM) images were obtained on a Tecnai G2 F30 microscope (FEI, America). X-ray diffraction (XRD) patterns were recorded by using a D8 Advance diffractometer (Bruker, Germany). Fourier-transform infrared (FT-IR) spectra were recorded on Spectrum one FT-IR spectrophotometer (Perkin Elmer, America). UV–vis absorption spectra (UV–vis) were performed on Lambda 35 UV spectrometer (Perkin Elmer,

**Scheme 1** Turn-off-on fluorescence sensing of citrate using  $\text{g-CNQDs}$  and  $\text{MgFe-LDH}$ .



America). The fluorescence measurements were recorded on LS55 fluorescence spectrometer (Perkin Elmer, America). Zeta potentials were measured on Zetasizer Nano ZS90 (Malvern, England).

### Synthesis of g-CNQDs

The g-CNQDs were prepared by Fan's method with minor modification [36]. First, 0.126 g (1 mmol) melamine and 0.248 g (0.67 mmol) EDTA were mixed in an agate mortar and grounded to uniform power, then put them into a ceramic crucible with a cover and heated at 350 °C for 1 h in air. Next, the obtained solid was dispersed in 30 mL of ultrapure water and formed a homogeneous brownish-black solution, and centrifuged (8000 rpm, 20 min) to remove the large particles. Finally, the purified g-CNQDs solution was obtained by dialyzing for 2 days.

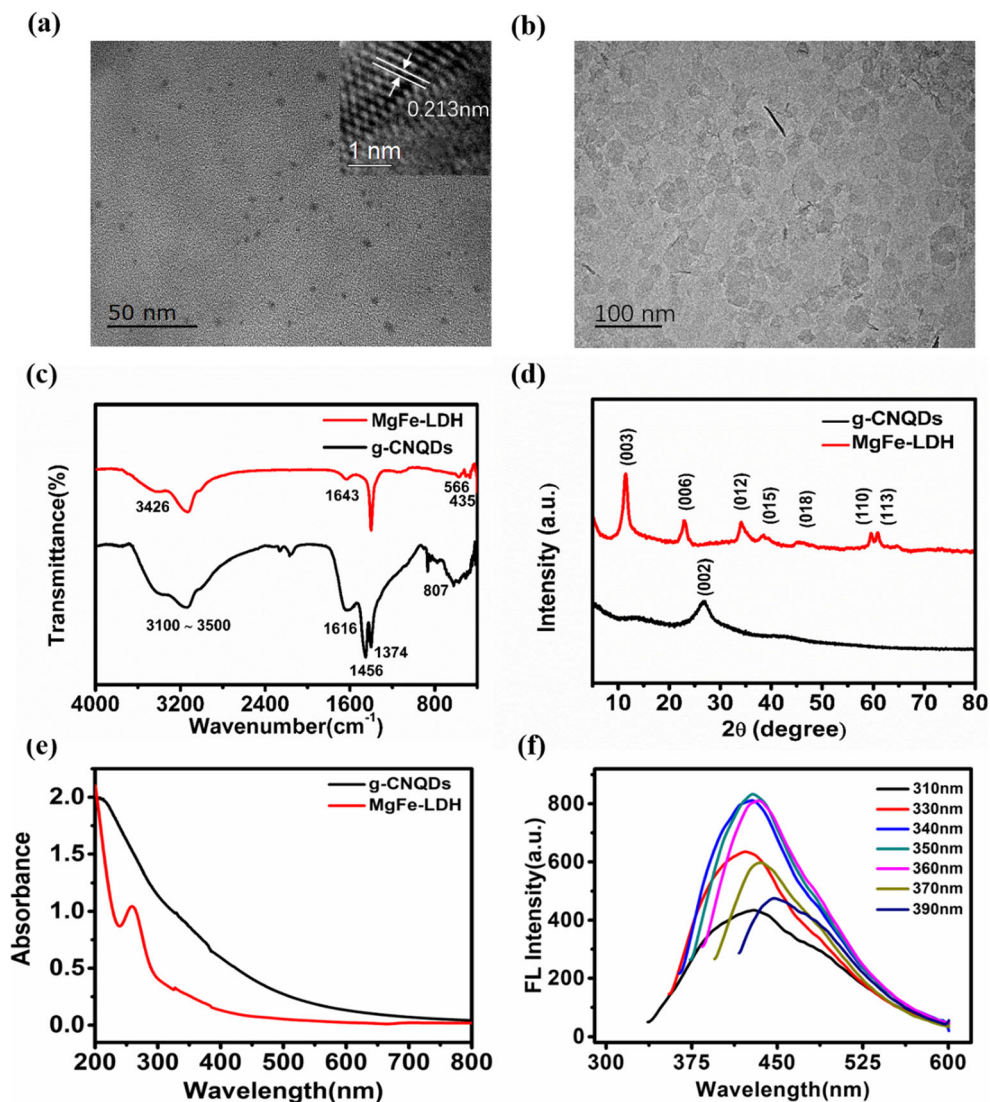
### Synthesis of MgFe-LDH

The MgFe-LDH was synthesized using a co-precipitation method [37]. First, NaOH solution (10 M, 0.4 mL) was added to 25 mL of premixed solution containing MgCl<sub>2</sub> (42 mM) and FeCl<sub>3</sub> (20 mM) and stirred for 15 min. Then, MgFe-LDH solid was obtained via centrifugation after washed 3 times with ultrapure water. The final product was dispersed in 25 mL ultrapure water under sonication, resulting in a stable homogeneous suspension.

### Analysis of Citrate in Aqueous Solution

In a typical assay, 10 μL of MgFe-LDH dispersion (3.5 mg mL<sup>-1</sup>) was mixed with 23.3 μL of the g-CNQDs solution. Then, different amounts of citrate were added to the mixture. Finally, mixture was diluted to 2 mL with water

**Fig. 1** **a** TEM and HRTEM image of g-CNQDs, **b** TEM image of MgFe-LDH. The FT-IR (**c**) and XRD spectra (**d**) of g-CNQDs and MgFe-LDH. **e** UV-vis absorption spectra of g-CNQDs (black) and MgFe-LDH (red). **f** Emission spectra of g-CNQDs



(pH = 6.0) and thoroughly mixed. Then the fluorescence intensity was measured at 435 nm with excitation at 350 nm after an incubation of 3 min at room temperature.

## Results and Discussion

### Characterization of g-CNQDs and MgFe-LDH

The TEM image and HRTEM image show that the as-prepared g-CNQDs are spherical and the lattice spacing is 0.213 nm (Fig. 1a and inset of Fig. 1a). Figure 1b illustrates that MgFe-LDH are the typical hexagon nanosheets morphology. The surface functional groups of the g-CNQDs and MgFe-LDH were characterized by FT-IR spectra (Fig. 1c). For g-CNQDs, the broad peak at 3100–3500  $\text{cm}^{-1}$  is assigned to O-H and N-H stretching. The peaks at 1456  $\text{cm}^{-1}$  and 1374  $\text{cm}^{-1}$  are assigned to stretching modes of CN heterocycles, and the peak at 807  $\text{cm}^{-1}$  is attributed to typical vibration of triazine units. The peak at 1616  $\text{cm}^{-1}$  is corresponded to the asymmetric stretching vibrations of the  $\text{COO}^-$ , suggesting the g-CNQDs are decorated with carboxylate and hydroxyl groups on the surface. For MgFe-LDH, the broad peaks around 3426  $\text{cm}^{-1}$  and 1643  $\text{cm}^{-1}$  correspond to stretching and bending vibrations of O-H, respectively. The peaks around 566 and 435  $\text{cm}^{-1}$  are assigned to lattice Mg-O and Fe-O vibrations. XRD patterns are determined in Fig. 1d. The

broad peak at 27.1° (002) is corresponded to the interlayer stacking of g-CNQDs. For MgFe-LDH, the pattern displays several sharp symmetry peaks at 11.4° (003), 22.9° (006), 34.1° (012), 59.5° (110) and 60.9° (113), the positions and relative intensities match well with previous report, indicating the existence of MgFe-LDH.

The optical properties of g-CNQDs and MgFe-LDH were further studied by UV-vis absorption and fluorescence spectra. As shown in Fig. 1e, both g-CNQDs and MgFe-LDH exhibit a very broad UV absorption between 200 and 500 nm, meanwhile MgFe-LDH has an absorption peak around 260 nm. The emission peaks of g-CNQDs are excitation-dependent and the maximum fluorescence emission is at 435 nm with an excitation of 350 nm (Fig. 1f).

### Feasibility of g-CNQDs for the Detection of Citrate

To explore the potential of the g-CNQDs for fluorescence detection of citrate, we investigated the effect of MgFe-LDH and citrate on the fluorescence of the g-CNQDs. As shown in Fig. 2a, the fluorescence intensity of g-CNQDs at 435 nm (black curve of Fig. 2a) is significantly quenched with the addition of MgFe-LDH (red curve of Fig. 2a). However, the quenched fluorescence of g-CNQDs is recovered upon the addition of citrate (blue curve of Fig. 2a). Therefore, we can establish a new platform for the fluorescence “turn-off-on” sensor for the detection of citrate.

**Fig. 2** a Fluorescence emission spectra of g-CNQDs, g-CNQDs/MgFe-LDH and g-CNQDs/MgFe-LDH in the presence of citrate (20  $\mu\text{L}$  g-CNQDs + 18  $\mu\text{g mL}^{-1}$  MgFe-LDH + 50  $\mu\text{M}$  citrate). Effects of (b) concentration of MgFe-LDH and (c) pH on the detection of citrate, where  $F_0$  and  $F$  refer to the fluorescence intensity of free g-CNQDs and g-CNQDs in the presence of MgFe-LDH and citrate, respectively. d The fluorescence intensity upon additions of different citrate concentrations during a period of 10 min

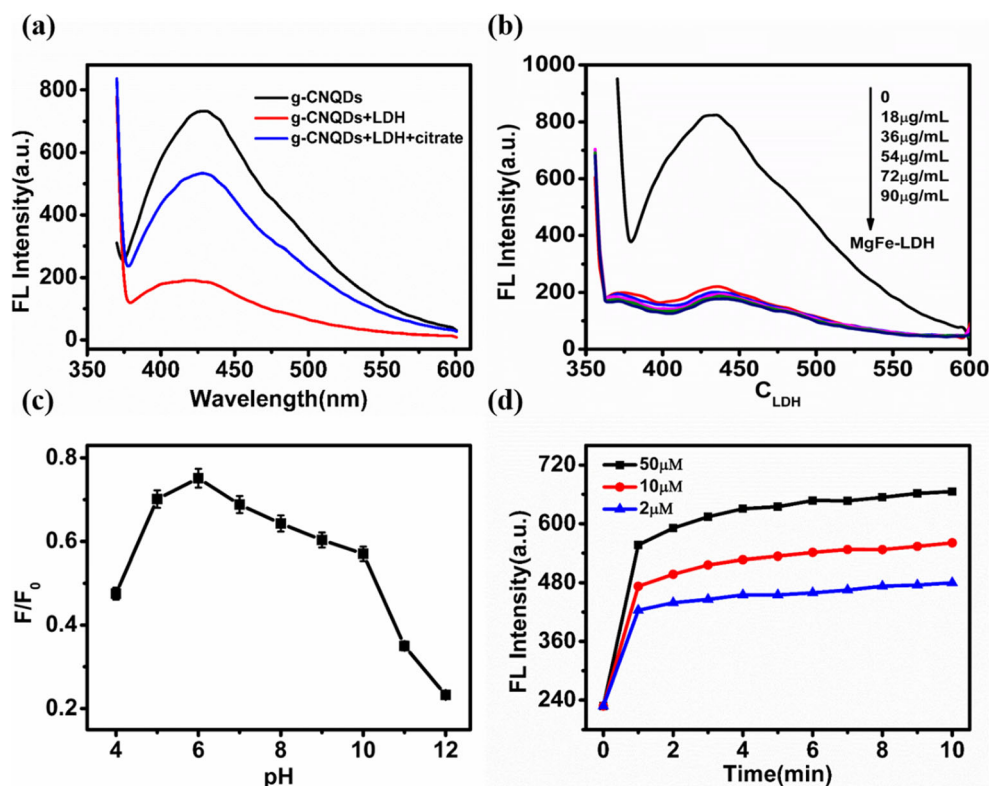
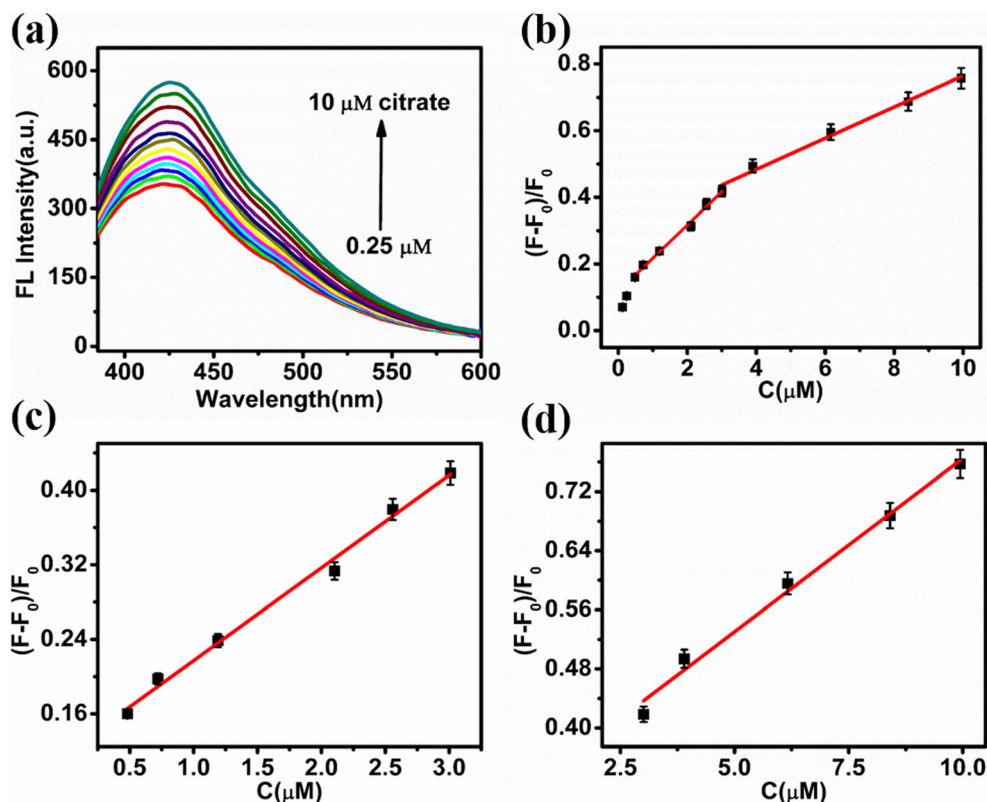




**Fig. 3** **a** Fluorescence spectra of g-CNQDs/MgFe-LDH in the presence of different concentrations of citrate. **b** Fluorescence responses of g-CNQDs/MgFe-LDH toward citrate. **c** The relationship between  $(F - F_0)/F_0$  and the concentration of citrate in the range from 0.5 to 3.0  $\mu\text{M}$  (d) and 3.0 to 10.0  $\mu\text{M}$ .  $F_0$  and  $F$  are fluorescence intensities without and with citrate, respectively. Error bars represent standard deviations from triplicate measurements



For the further sensing assay, we optimized detection condition including the concentration of MgFe-LDH, pH and reaction time. The fluorescence quenching of g-CNQDs upon different concentration of MgFe-LDH was investigated. As shown in Fig. 2b, the fluorescence of g-CNQDs is decreased rapidly when  $18 \mu\text{g mL}^{-1}$  of MgFe-LDH are added. Here, we chose  $18 \mu\text{g mL}^{-1}$  of MgFe-LDH for the experiment. Figure 2c displays the influence of pH on the recovery of fluorescence. The results show that the change of pH values significantly affect the recovery of the fluorescence of g-CNQDs and the optimum pH to reach greatest recovery in this study is 6.0. Herein, we use  $F/F_0$  value to evaluate the effects, where  $F_0$  and  $F$

refer to the fluorescence intensity of free g-CNQDs and g-CNQDs in the presence of MgFe-LDH and citrate, respectively. Figure 2d demonstrates the fluorescence enhancement kinetics with different amounts of citrate addition. The fluorescence intensity of g-CNQDs recovers quickly in 3 min, indicating it is fast to reach equilibrium in the interaction between citrate and g-CNQDs/MgFe-LDH. Thus, the detection experiments were carried out in 3 min.

To evaluate the sensitivity of the g-CNQDs for the fluorescence detection of citrate, the fluorescence intensity of the g-CNQDs at 435 nm is monitored as a function of the

**Table 1** Comparison of different methods for the determination of citrate

Materials used	Analytical range	Detection limit	References
CdTe QDs	0.67–133 $\mu\text{M}$	60 nM	[13]
Receptor 1	0.1–0.5 $\mu\text{M}$	180 nM.	[14]
Dinuclear zinc complex	0–10 $\mu\text{M}$	100 nM	[15]
Rhodamine compound	0.1–50 $\mu\text{M}$	25 nM	[16]
DPP-Py1	0–40 $\mu\text{M}$	180 nM	[17]
TPE-Py	1–5 $\mu\text{M}$	100 nM	[18]
g-CNQDs/MgFe-LDH	0.5–10 $\mu\text{M}$	12.3 nM	This paper

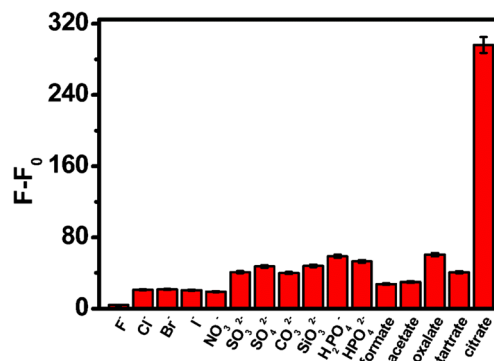


**Fig. 4** The selectivity of g-CNQDs/MgFe-LDH nanoprobe for citrate detection. The concentration of different anions are 10  $\mu\text{M}$ . Where  $F$  and  $F_0$  are the fluorescence intensities at 435 nm in the presence and absence of anions, respectively

**Table 2** Analytical results of citrate in urine samples ( $n = 3$ )

Samples	Spiked ( $\mu\text{M}$ )	Found ( $\mu\text{M}$ )	Recovered (%)	RSD (%)
1	1.0	$1.00 \pm 0.01$	99.8	0.89
	2.0	$2.05 \pm 0.07$	102.5	3.63
	5.0	$5.09 \pm 0.05$	101.9	1.03
2	1.0	$1.03 \pm 0.06$	102.9	5.68
	2.0	$2.03 \pm 0.04$	101.4	1.73
	5.0	$5.00 \pm 0.05$	99.9	1.01

concentration of citrate (Fig. 3). As shown in Fig. 3a, the fluorescence intensity of g-CNQDs/MgFe-LDH is gradually enhanced with increasing concentration of citrate. The linear calibration ranges are obtained within 0.5–3.0  $\mu\text{M}$  and 3.0–10.0  $\mu\text{M}$  (Fig. 3b). Figure 3c and d display the linear relationships between  $(F-F_0)/F_0$  and citrate concentration, with regressions equation of  $(F-F_0)/F_0 = 0.010C + 0.118$  ( $R^2 = 0.992$ ) and  $(F-F_0)/F_0 = 0.047C + 0.296$  ( $R^2 = 0.987$ ), respectively. Herein,  $F_0$  and  $F$  were the fluorescence intensity of the g-CNQDs/MgFe-LDH at 435 nm in the absence and presence of citrate. The limit of detection (LOD) of 12.3 nM is calculated based on  $3\sigma/k$  ( $\sigma$  is the standard deviation of blank signal ( $S/N=3$ ) and  $k$  is the slope of calibration curve. Table 1 shows a comparison of merits of some reported methods for citrate determination with our method.

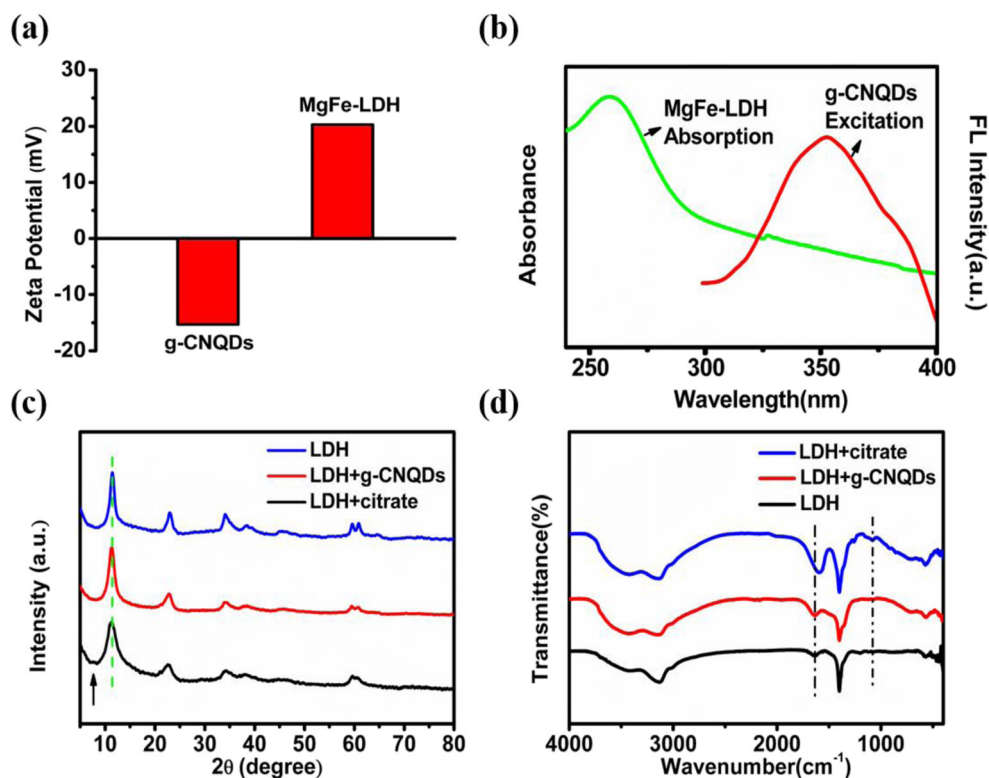
### Selectivity of g-CNQDs/MgFe-LDH Based Method for the Detection of Citrate

The selectivity of the g-CNQDs/MgFe-LDH based method for the detection of citrate was evaluated, some interfering anions ( $\text{F}^-$ ,  $\text{Cl}^-$ ,  $\text{Br}^-$ ,  $\text{I}^-$ ,  $\text{NO}_3^-$ ,  $\text{CO}_3^{2-}$ ,  $\text{SO}_3^{2-}$ ,  $\text{SO}_4^{2-}$ ,  $\text{SiO}_3^{2-}$ ,  $\text{H}_2\text{PO}_4^-$ ,  $\text{HPO}_4^{2-}$ , formate, acetate, oxalate and tartrate) were employed as control samples. As shown in Fig. 4, only the addition of citrate exhibits a significant response on the fluorescence intensity of g-CNQDs/MgFe-LDH. These results demonstrate that the proposed method is highly selective for distinguishing citrate from other anions. To further evaluate the selectivity of the present method, a coexisting experiment was performed. The results show that the presence of 50  $\mu\text{M}$  of interference substances has little influence on 10  $\mu\text{M}$  citrate detection, the relative error caused by the coexisting substances was less than  $\pm 5\%$ .

### Detection of the Citrate Levels in Human Urine Samples

To further investigate the potential practical applications of this method, the sensing of citrate in human urine was carried out. In this work, the human urine samples were diluted 100 times with water just before determination without further pretreatment. The assay results were displayed in Table 2, the recovery of citrate is ranging from 99.8% to 102.9% with

**Fig. 5** **a** Zeta potential of g-CNQDs and MgFe-LDH, **b** UV-vis absorption spectra of MgFe-LDH (green) and excitation spectra of the g-CNQDs (red). XRD patterns (**c**) and FT-IR spectra (**d**) of MgFe-LDH, MgFe-LDH in the presence of g-CNQDs (LDH + g-CNQDs) and MgFe-LDH in the presence of citrate (LDH + citrate)



the RSD values less than 5.7%. These results confirm that the reported method is suitable for detection of citrate in real samples.

### Possible Mechanism of the g-CNQDs for the Fluorescence “Turn-off-on” Detection of Citrate

The zeta potential of g-CNQDs and MgFe-LDH are  $-17.3$  mV and  $20.4$  mV, respectively (Fig. 5a). Therefore, g-CNQDs interact with MgFe-LDH via electrostatic interaction. The UV-vis absorption spectra and fluorescence spectra were tested to investigate the causes of fluorescence quenching. As it can be seen in Fig. 5b, the characteristic absorption band of MgFe-LDH between 200 and 400 nm can well overlap with the excitation spectrum of g-CNQDs at 350 nm, thus enabling the generation of the inner filter effect between g-CNQDs and MgFe-LDH, the fluorescence of g-CNQDs is significantly quenched by MgFe-LDH via inner filter effect. For the classic intercalation between LDH and citrate, the citrate competes with negatively charged g-CNQDs to form fairly stable complexes with MgFe-LDH. Thus, the fluorescence of g-CNQDs is recovered due to replacement of g-CNQDs by citrate.

The XRD and FT-IR were employed to demonstrate the formation of complexes between citrate and MgFe-LDH. The XRD pattern of g-CNQDs/MgFe-LDH is in consistent with the pure MgFe-LDH, indicating the structure of MgFe-LDH is not destroyed after the electrostatic interaction between g-CNQDs and MgFe-LDH. While the (003) peak of MgFe-LDH becomes broader and a new peak appears at lower angle after interaction with citrate, which indicates citrate can be partially intercalated in the layered structures of MgFe-LDH (Fig. 5c). In the FT-IR spectra (Fig. 5d), the symmetric vibration peak of C=O at  $1592\text{ cm}^{-1}$  and the peak C-O bond at  $1079\text{ cm}^{-1}$  of citrate is appeared in the complex of citrate and MgFe-LDH, which suggests citrate binding with MgFe-LDH through the carboxyl group. Hence, the structure information of MgFe-LDH before and after interaction with citrate offer possible mechanism of the g-CNQDs for the fluorescence “turn-off-on” detection of citrate.

### Conclusions

In summary, we successfully synthesized g-CNQDs and MgFe-LDH, respectively. The g-CNQDs interacted with MgFe-LDH through electrostatic interaction. Since the absorption band of MgFe-LDH between 200 and 400 nm could well overlap with the excitation spectrum of g-CNQDs at 350 nm, the fluorescence of g-CNQDs was significantly quenched by MgFe-LDH via inner filter effect. After the addition of citrate, the citrate would compete with g-CNQDs and

form fairly stable complexes with MgFe-LDH because of the intercalation between MgFe-LDH and citrate. As a result, the g-CNQDs was replaced by citrate and the fluorescence of g-CNQDs was recovered. Based on these findings, we constructed a g-CNQDs-based sensor for “turn-off-on” detection for citrate. The established method achieved satisfying results for citrate detection with linear range of  $0.5\text{--}3.0\text{ }\mu\text{M}$  and  $3.0\text{--}10.0\text{ }\mu\text{M}$ . Moreover, this method was applied to determine the citrate level in human urine samples and exhibited satisfactory results, which demonstrated its potential for practical diagnostic applications.

**Acknowledgments** This work was financially supported by National Natural Science Foundation of China (21707030) and Wuhan Youth Science and technology plan (2016070204010133).

### References

1. Wise DR, Ward PS, Shay JES, Cross JR, Gruber JJ, Sachdeva UM, Platt JM, DeMatteo RG, Simon MC, Thompson CB (2011) Hypoxia promotes isocitrate dehydrogenase-dependent carboxylation of  $\alpha$ -ketoglutarate to citrate to support cell growth and viability. *Proc Natl Acad Sci U S A* 108:19611–19616
2. Hatzivassiliou G, Zhao FD, Andreadis C, Shaw AN, Dhanak D, Hingorani SR et al (2005) Atp citrate lyase inhibition can suppress tumor cell growth. *Cancer Cell* 8:311–321
3. Costello LC, Franklin RB (2006) The clinical relevance of the metabolism of prostate cancer; zinc and tumor suppression: connecting the dots. *Mol Cancer* 5:17
4. Muñoz JA, López-Mesas M, Valiente M (2010) Development and validation of a simple determination of urine metabolites (oxalate, citrate, uric acid and creatinine) by capillary zone electrophoresis. *Talanta* 81:392–397
5. Cebotaru V, Kaul S, Devuyt O, Cai H, Racusen L, Guggino WB, Guggino SE (2005) High citrate diet delays progression of renal insufficiency in the CIC-5 knockout mouse model of Dent's disease. *Kidney Int* 68:642–652
6. Schell-Feith EA, Maerdijk A, Zweiten PHTV, Zanderland HM, Holscher HC, Holthe JK, van der Heijden BJ (2006) Does citrate prevent nephrocalcinosis in preterm neonates? *Pediatr.Nephrol.* 21: 1830–1836
7. DeBorba BM, Rohrer JS, Bhattacharyya L (2004) Development and validation of an assay for citric acid/citrate and phosphate in pharmaceutical dosage forms using ion chromatography with suppressed conductivity detection. *J Pharm Biomed Anal* 36:517–524
8. Chalgeri A, Tan HS (1996) Indirect photometric detection for determination of citrate in pharmaceutical matrices by ion chromatography. *J Pharm Biomed Anal* 14:835–844
9. Kelebek H, Selli S, Canbas A, Cabaroglu T (2009) HPLC determination of organic acids, sugars, phenolic compositions and antioxidant capacity of orange juice and orange wine made from a Turkish cv. Kozan, *Microchem J* 91:187–192
10. Miyakoshi K, Komoda M (1977) Determination of citric acid and its decomposed products in edible oils by gas liquid chromatography. *J Am Oil Chem Soc* 54:331–339
11. Capitan-Vallvey LF, Arroyo-Guerrero E, Fernandez-Ramos MD, Santoyo-Gonzalez F (2005) Development of a one-shot optical citrate sensor based on a guanidinium synthetic receptor. *Microchim Acta* 151:93–100

12. Trabesinger AH, Meier D, Dydak U, Lamerichs R, Boesiger P (2005) Optimizing press localized citrate detection at 3 tesla. *Magn Reson Med* 54:51–58
13. Zhuo S, Gong J, Ping Z, Zhu C (2015) High-throughput and rapid fluorescent visualization sensor of urinary citrate by cdte quantum dots. *Talanta* 141:21–25
14. Liu ZH, Devaraj S, Yang CR, Yen YP (2012) A new selective chromogenic and fluorogenic sensor for citrate ion. *Sensors Actuators B Chem* 174:555–562
15. Zhu Z, Zhou J, Li Z, Yang C (2015) Dinuclear zinc complex for fluorescent indicator-displacement assay of citrate. *Sensors Actuators B Chem* 208:151–158
16. Li CY, Zhou Y, Li YF, Kong XF, Zou CX, Weng C (2013) Colorimetric and fluorescent chemosensor for citrate based on a rhodamine and pb<sup>2+</sup> complex in aqueous solution. *Anal Chim Acta* 774:79–84
17. Hang Y, Jian W, Tao J, Lu N, Hua J (2016) Diketopyrrolopyrrole-based ratiometric/turn-on fluorescent chemosensors for citrate detection in the near-infrared region by an aggregation-induced emission mechanism. *Anal Chem* 88:1696–1703
18. Liu C, Hang Y, Jiang T, Yang J, Zhang X, Hua J (2018) A light-up fluorescent probe for citrate detection based on bispyridinium amides with aggregation-induced emission feature. *Talanta* 178:847–853
19. Ding YD, Tong ZW, Nan YH, Wang YJ, Zou XY, Jiang ZY (2017) Graphitic carbon nitride-based nanocomposites as visible-light driven photocatalysts for environmental purification. *Environ Sci* 4:1455–1469
20. Oh J, Yoo RJ, Kim SY, Lee YJ, Kim DW, Park S (2015) Oxidized carbon nitrides: water-dispersible, atomically thin carbon nitride-based Nanodots and their performances as bioimaging probes. *Chem-Eur J* 21:6241–6246
21. Chen LC, Song JB (2017) Tailored graphitic carbon nitride nanostructures: synthesis, modification, and sensing applications. *Adv Funct Mater* 27:1702695
22. Xiong M, Rong Q, Meng HM, Zhang XB (2016) Two-dimensional graphitic carbon nitride nanosheets for biosensing applications. *Biosens Bioelectron* 89:212–223
23. Huang H, Chen R, Ma J, Yan L, Zhao Y, Wang Y, Zhang W, Fan J, Chen X (2014) Graphitic carbon nitride solid nanofilms for selective and recyclable sensing of Cu<sup>2+</sup> and ag<sup>+</sup> in water and serum. *Chem Commun* 50:15415–15418
24. Zhang S, Li J, Zeng M, Xu J, Wang X, Hu W (2014) Polymer nanodots of graphitic carbon nitride as effective fluorescent probes for the detection of Fe<sup>3+</sup> and Cu<sup>2+</sup> ions. *Nanoscale* 6:4157–4162
25. Xu YL, Niu XY, Zhang HJ, Xu LF, Zhao SG, Chen HL, Chen XG (2015) Switch-on fluorescence sensing of glutathione in food samples based on a (g-CNQD)-Hg<sup>2+</sup> chemo-sensor. *Agric Food Chem* 63:1747–1755
26. Tang Y, Song H, Su Y, Lv Y (2013) Turn-on persistent luminescence probe based on graphitic carbon nitride for imaging detection of biothiols in biological fluids. *Anal Chem* 85:11876–11884
27. Yan L, Zhou MJ, Zhang XJ, Huang LB, Chen W, Roy VAL, Zhang W, Chen X (2017) A novel type of aqueous dispersible ultrathin layered double hydroxide nanosheets for in vivo bioimaging and drug delivery. *ACS Appl Mater Interfaces* 9:34185–34193
28. Zhang P, Hu Y, Li L, Lu J (2017) Enhanced green fluorescence protein/layered double hydroxides composite ultrathin film: bio-hybrid assembly and its potential application as a fluorescent biosensor. *J Mater Chem B* 5:160–166
29. He R, Li M, Fu Y, Jin L (2016) Silver nanoclusters functionalized by chromotropic acid and layered double hydroxides for turn-on detection of melamine. *J Mater Chem C* 4:6104–6109
30. Song L, Shi W, Chao L (2016) Confinement effect in layered double hydroxide nanoreactor: improved optical sensing selectivity. *Anal Chem* 88:8188–8193
31. Liu JY, Lv GC, Gu WL, Li ZH, Tang AW, Mei LF (2017) A novel luminescence probe based on layered double hydroxides loaded with quantum dots for simultaneous detection of heavy metal ions in water. *J Mater Chem C* 5:5024–5030
32. Li M, Fu Y, Jin L (2017) A dual-signal sensing system based on organic dyes-lhds film for fluorescence detection of cysteine. *Dalton Trans* 46:7284–7290
33. Zhang XL, Zheng C, Guo SS, Li J, Yang H, Chen GN (2014) Turn-on fluorescence sensor for intracellular imaging of glutathione using g-C<sub>3</sub>N<sub>4</sub> nanosheet-MnO<sub>2</sub> sandwich nanocomposite. *Anal Chem* 86:3426–3434
34. Liu JJ, Tang DS, Chen ZT, Yan XM, Zhong Z, Kang LT, Yao JN (2017) Chemical redox modulated fluorescence of nitrogen-doped graphene quantum dots for probing the activity of alkaline phosphatase. *Biosens Bioelectron* 94:271–277
35. Ma JL, Yin BC, Wu X, Ye BC (2017) Simple and cost-effective glucose detection based on carbon Nanodots supported on silver nanoparticle. *Anal Chem* 89:1323–1328
36. Fan XQ, Feng Y, Su YY, Zhang LC, Lv Y (2015) A green solid-phase method for preparation of carbon nitride quantum dots and their applications in chemiluminescent dopamine sensing. *RSC Adv* 5:55158–55164
37. Shan Z, Lu M, Curry DE, Beale S, Campbell S, Poduska KM et al (2017) Regenerative nanobots based on magnetic layered double hydroxide for azo dye removal and degradation. *Chem Commun* 53:10456–10458

**Publisher's Note** Springer Nature remains neutral with regard to jurisdictional claims in published maps and institutional affiliations.